

Identical-Particle Symmetry-Enabled Complete Coherent Control of Ultracold Atomic and Molecular Collisions

Jing-Chen Zhang(张京晨),^{1,2,3,4,*} Adrien Devolder,^{5,†} Timur V. Tschersbul,^{6,‡} Paul Brumer,^{5,§} and Yu Liu^{1,2,3,¶}

¹*Institute for Physical Science and Technology, University of Maryland, College Park, Maryland 20742, USA*

²*Department of Chemistry and Chemical Biology,*

University of Maryland, College Park, Maryland 20742, USA

³*Joint Quantum Institute, University of Maryland and National Institute of Standards and Technology (NIST), College Park, Maryland 20742, USA*

⁴*Joint Center for Quantum Information and Computer Science, University of Maryland, College Park, Maryland 20742, USA*

⁵*Chemical Physics Theory Group, Department of Chemistry, and Center for Quantum Information and Quantum Control, University of Toronto, Toronto, Ontario M5S 3H6, Canada*

⁶*Department of Physics, University of Nevada, Reno, Nevada 89557, USA*

(Dated: July 3, 2026)

We show that exchange symmetry in collisions of identical particles enables symmetry-protected coherent control of the total scattering cross section. For identical fermions, antisymmetrization enforces complete phase synchronization of the contributing scattering channels, yielding maximal control visibility. For identical bosons, synchronization persists but with reduced visibility due to additional exchange (satellite) contributions. Collisions of distinguishable particles lack this symmetry-imposed phase locking, leading to lower controllability and visibility. We elucidate these principles through coupled-channel quantum-scattering calculations for lithium–lithium collisions, comparing the ${}^6\text{Li}$ – ${}^6\text{Li}$ (identical fermions), ${}^7\text{Li}$ – ${}^7\text{Li}$ (identical bosons), and ${}^6\text{Li}$ – ${}^7\text{Li}$ (distinguishable) systems. Furthermore, in the identical particle cases, symmetry-enforced synchronization enables full control over the parity of the final state at any collisional energy. This mechanism is broadly applicable to identical-particle collisions, including homonuclear molecules for which established approaches—DC electric fields, or microwave shielding—are ineffective or unavailable.

Introduction. Over the past few decades, advances in quantum technology have enabled precise preparation, control, and detection of ultracold atoms and molecules [1–5]. External fields, especially magnetic Feshbach resonances, routinely tune atomic scattering with high precision [6]. While such resonances have also been observed in ultracold molecule-molecule collisions [7], comparable control for these collisions remains challenging. Nevertheless, state-resolved preparation and detection are increasingly viable, bringing molecular collisions to the forefront of ultracold chemistry and quantum science [8–10].

A central challenge is controlling ultracold bimolecular chemical reactions such as $\text{KRb} + \text{KRb} \rightarrow \text{K}_2 + \text{Rb}_2$ [11, 12], whose many internal and relative-motion degrees of freedom make full-dimensional quantum scattering intractable [13]. At short range, dense resonances and many exit channels mean that controlling the *total* cross section demands phase coherence across different scattering channels. Superposition-based coherent control [14, 15] can steer particular state-to-state channels, but the total cross section is usually insensitive: non-interfering “satellite” terms from the superposition components [14] and short-range internal state/partial-wave scrambling wash out interference when summing over final states [16]. Entanglement can suppress the satellite background [17], but phase scrambling across final channels remains the main obstacle.

Existing strategies regain control by restricting interference pathways. Symmetry-based methods exploit selection rules (e.g., nuclear-spin sectors), often assuming short-range nuclear-spin conservation [18, 19], or the use of time-reversal-invariant eigenstates [20]. For polar molecules, microwave dressing generates repulsive adiabatic potentials that suppress access to the short-range region and reduce inelastic and reactive losses [21–23]. Double microwave shielding further enhances this suppression and has recently enabled molecular Bose–Einstein condensation [24–26]. However, nuclear-spin conservation is not guaranteed in complex-forming collisions [27], and microwave shielding requires a permanent electric dipole, excluding homonuclear molecules.

Thus, a general control strategy for coherent control of the total cross section in collisions of identical ultracold particles remains missing. This is particularly appealing because the total cross section is experimentally accessible and provides a natural observable for the first demonstrations of coherent control in bimolecular collisions [28–30]. The coherent control of the total cross section is described by the coherent multichannel optical theorem [30], which specifies conditions for full coherent control in terms of the imaginary parts of forward-scattering amplitudes. However, it does not reveal the underlying physical mechanisms that allow these conditions to be met.

Here we show that identical-particle exchange symme-

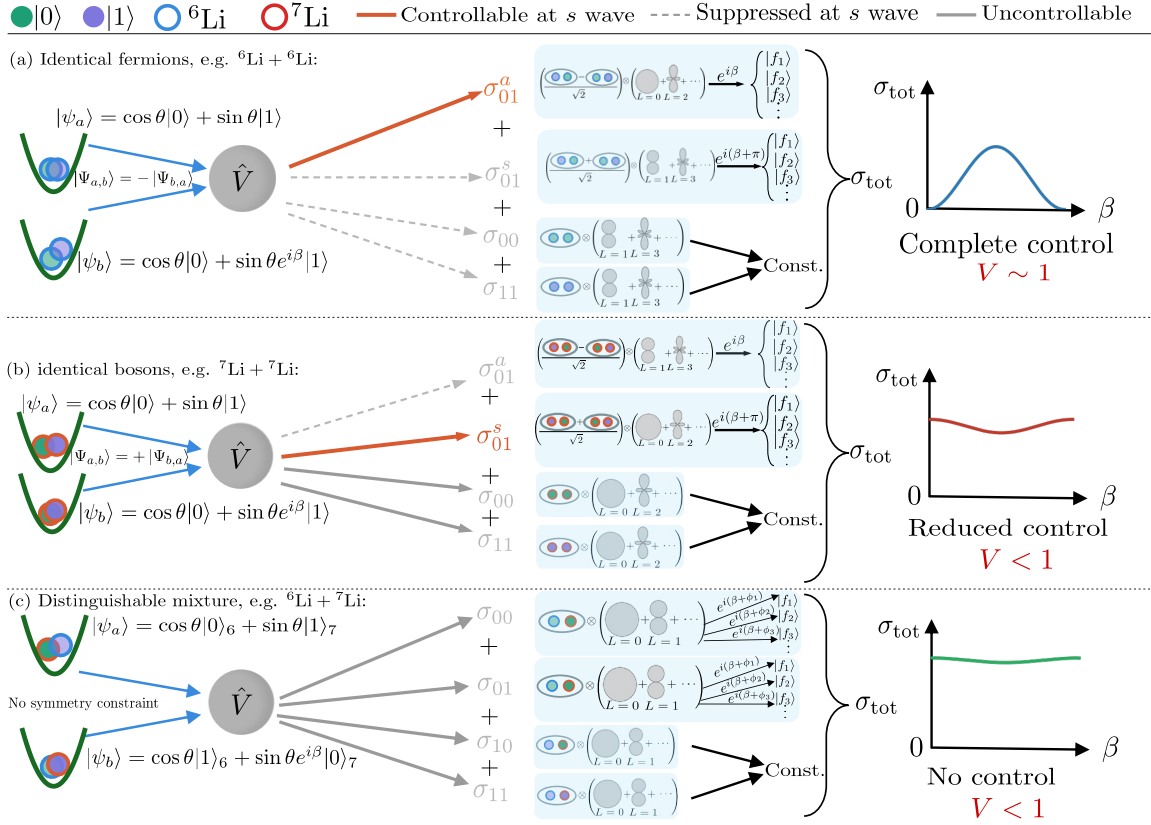


FIG. 1: Exchange-symmetry-enabled coherent control of the total cross section σ_{tot} for (a) identical fermions (${}^6\text{Li}+{}^6\text{Li}$), (b) identical bosons (${}^7\text{Li}+{}^7\text{Li}$), and (c) a distinguishable mixture (${}^6\text{Li}+{}^7\text{Li}$). *Left*: the atoms are prepared in the superpositions $|\psi_a\rangle$, $|\psi_b\rangle$ of Eqs. (1)–(2), collide via \hat{V} . *Middle*: each two-particle internal state scatters through its symmetry-allowed partial waves L into the final channels $\{|f_i\rangle\}$; summing the state-to-state cross sections over these channels gives that sector’s contribution to σ_{tot} . *Right*: the exchange-symmetry constraints on the available channels set the resulting $\sigma_{\text{tot}}(\beta)$ and control visibility V for each case.

try provides a mechanism by synchronizing short-range phase shifts across exit channels within a given exchange-parity sector (Fig. 1). As a result, quantum interference underlying coherent control [14] survives summation over final states at ultracold temperatures, enabling control of the total cross section despite complex short-range dynamics. We find maximal visibility for identical fermions, reduced visibility for identical bosons due to residual satellite contributions, and none for distinguishable particles. For ultracold ${}^6\text{Li}-{}^6\text{Li}$, ${}^7\text{Li}-{}^7\text{Li}$, and ${}^6\text{Li}-{}^7\text{Li}$ collisions, tailored internal superpositions control exchange-parity populations and thus scattering outcomes. This is particularly promising for nonpolar or weakly polar molecules such as ${}^6\text{Li}{}^7\text{Li}+{}^6\text{Li}{}^7\text{Li}$ or Sr_2+Sr_2 , where dipole-enabled shielding is unavailable.

Limitation of coherent control of non-identical particles. Scrambling arising from conflicts between individual control pathways is a fundamental limitation of coherent control in collisions [16, 31]. To clarify its origin and how exchange symmetry can mitigate it, we first consider collisions of non-identical particles, where molecules

A and B are independently prepared in coherent superpositions of two internal eigenstates, $|0\rangle$ and $|1\rangle$:

$$\Psi_1 = \cos\theta|0\rangle_A + \sin\theta|1\rangle_A \quad (1)$$

$$\Psi_2 = \cos\theta|0\rangle_B + \sin\theta e^{i\beta}|1\rangle_B \quad (2)$$

with a controllable relative phase β introduced between the two molecules. Quantum interference requires degenerate internal states; otherwise, $|0\rangle_A|1\rangle_B$ and $|1\rangle_A|0\rangle_B$ are energetically distinguishable and do not interfere [32]. In practice, this is often achieved using superpositions of states with the same internal angular momentum but different projections, i.e., m -superpositions [33].

The corresponding total internal state of the two-molecule system can be expressed as the tensor product of the individual states: $\Psi_{\text{ini}} = \cos^2\theta|0\rangle_A|0\rangle_B + \cos\theta\sin\theta e^{i\beta}|0\rangle_A|1\rangle_B + \cos\theta\sin\theta|1\rangle_A|0\rangle_B + \sin^2\theta e^{i\beta}|1\rangle_A|1\rangle_B$. Alternatively, one can prepare entangled superpositions: $\Psi_{\text{ini}} = \cos\theta|0\rangle_A|1\rangle_B + \sin\theta e^{i\beta}|1\rangle_A|0\rangle_B$, which avoid population in the uncontrolled satellite states $|0\rangle_A|0\rangle_B$

and $|1\rangle_A |1\rangle_B$ and are expected to offer enhanced controllability [15, 17]. Although such entangled molecular states have recently been realized [34–36], they remain experimentally challenging. We therefore focus on product states, with entangled-state results given in the Supplementary Material [37].

The total scattering cross section can be written as $\sigma = \mathbf{a}^\dagger \mathbf{C} \mathbf{a}$ [38, 39], where $\mathbf{a} = (\cos^2 \theta, \cos \theta \sin \theta e^{i\beta}, \cos \theta \sin \theta, \sin^2 \theta e^{i\beta})$. The coherent control scattering (CCS) matrix \mathbf{C} is defined as

$$C_{ij} = \frac{\pi}{k^2} \sum_f \sum_{\ell, m} \sum_{\ell', m'} T_{i, \ell, m \rightarrow f, \ell', m'} T_{j, \ell, m \rightarrow f, \ell', m'}^* \quad (3)$$

in terms of $T_{i, \ell \rightarrow f, \ell'}$, the T -matrix elements connecting the initial internal state $|i\rangle$ in the initial partial wave (ℓ, m) to the final state $|f\rangle$ in the final partial wave (ℓ', m') . Here, m and m' are the projections of the partial wave states ℓ and ℓ' on the quantization axis, and k is the relative incident momentum. $|f\rangle = |f_1\rangle_A |f_2\rangle_B$, where $|f_1\rangle_A$ is an internal state of the molecule A and $|f_2\rangle_B$ is an internal state of the molecule B after the collision. The sum over final states includes the elastic channel as well as all inelastic transitions.

We note that nonvanishing interference requires equal total projection of the internal angular momentum and energy [40], so only the states $|0\rangle_A |1\rangle_B$ and $|1\rangle_A |0\rangle_B$ interfere. The resulting total cross section is:

$$\begin{aligned} \sigma^{\text{non-ident}}(\theta, \beta) &= \cos^4 \theta \sigma_{0,0} + \cos^2 \theta \sin^2 \theta \sigma_{0,1} \\ &\quad + \cos^2 \theta \sin^2 \theta \sigma_{1,0} + \sin^4 \theta \sigma_{1,1} \quad (4) \\ &\quad + 2 \sin^2 \theta \cos^2 \theta \sigma_{\text{int}}(\beta) \end{aligned}$$

where each σ is the diagonal element of the CCS matrix, e.g., $\sigma_{0,0} = \mathbf{C}_{00,00} = \frac{\pi}{k^2} \sum_f \sum_{\ell, m} \sum_{\ell', m'} |T_{00, \ell, m \rightarrow f, \ell', m'}|^2$. $\sigma_{\text{int}}(\theta, \beta)$ is the total interference term between $|01\rangle$ and $|10\rangle$ and is defined as:

$$\begin{aligned} \sigma_{\text{int}}(\beta) &= \sum_f \sum_{\ell, m, \ell', m'} |\sigma_{\text{int}, \ell, m \rightarrow f, \ell', m'}| \\ &\quad \times \cos(\beta + \Phi_{f, \ell, m, \ell', m'}) \quad (5) \end{aligned}$$

Here, $\sigma_{\text{int}, \ell, m \rightarrow f, \ell', m'} = \frac{\pi}{k^2} T_{01, \ell, m \rightarrow f, \ell', m'} T_{10, \ell, m \rightarrow f, \ell', m'}^*$ is the individual interference term for the specific final internal states $|f\rangle$ and partial waves (ℓ, m, ℓ', m') , and $\Phi_{f, \ell, m, \ell', m'}$ is the phase of $\sigma_{\text{int}, \ell, m \rightarrow f, \ell', m'}$.

Summing the contributions in Eq. (5) reduces controllability due to two scrambling mechanisms: phase averaging and path indistinguishability. If the phases $\Phi_{f, \ell, m, \ell', m'}$ are random, interference terms cancel upon summation, leading to dephasing and loss of control [16, 31]. Moreover, maximal interference requires indistinguishable pathways, but the ratio $\frac{|T_{01, \ell, m \rightarrow f, \ell', m'}|^2}{|T_{10, \ell, m \rightarrow f, \ell', m'}|^2}$ depends on the final state and partial waves, so no choice

of initial populations can enforce indistinguishability for all channels simultaneously.

Scrambling from summation over initial and final partial waves is termed partial-wave scrambling, while that from summing over final internal states is internal-state scrambling. At ultracold temperatures, the limited number of contributing partial waves reduces partial-wave scrambling [41], but internal-state scrambling remains and continues to limit control.

Coherent control of identical particles. These limitations from partial-wave and internal-state scrambling can be removed in ultracold collisions of identical particles via exchange symmetry, as shown below. Exchange symmetry locks the two-particle internal-state symmetry to the partial-wave parity, allowing only symmetry-allowed partial waves within each sector and constraining exchange-related scattering amplitudes to differ only by phases of 0 or π . As a result, the coherent-control interference term survives summation over final states and same-parity partial waves, enabling control of the total cross section.

Unlike the non-identical case, the single-particle states $|0\rangle$ and $|1\rangle$ in Eqs. (1) and (2) need not be degenerate [32], relaxing constraints on preparing m -superpositions. However, both particles must be prepared in the same pair of basis states; otherwise exchange symmetry is broken and channel-dependent phases reappear (see Supplementary Material [37]). For identical particles, it is convenient to rewrite the two-molecule state in symmetric and antisymmetric combinations of $|0\rangle |1\rangle$ and $|1\rangle |0\rangle$: $|0, 1\rangle_s = \frac{1}{\sqrt{2}} (|0\rangle |1\rangle + |1\rangle |0\rangle)$ and $|0, 1\rangle_a = \frac{1}{\sqrt{2}} (|0\rangle |1\rangle - |1\rangle |0\rangle)$. Using these definitions, the initial two-molecule state can be rewritten as $\Psi_{\text{ini}} = \cos^2 \theta |0\rangle |0\rangle + \frac{\sin \theta \cos \theta}{\sqrt{2}} (1 + e^{i\beta}) |0, 1\rangle_s + \frac{\sin \theta \cos \theta}{\sqrt{2}} (e^{i\beta} - 1) |0, 1\rangle_a + \sin^2 \theta e^{i\beta} |1\rangle |1\rangle$. The states $|0\rangle |0\rangle$, $|0, 1\rangle_s$ and $|1\rangle |1\rangle$ are symmetric under particle exchange. Consequently, fermionic molecules in these states scatter via odd partial waves, while bosonic molecules scatter via even partial waves. In contrast, the antisymmetric state $|0, 1\rangle_a$ scatters via even partial waves for fermions and odd partial waves for bosons.

Interference in the symmetrized basis is determined by the corresponding CCS matrix. It can occur only between states with identical internal energies, restricting it to $|0, 1\rangle_s$ and $|0, 1\rangle_a$. However, the CCS matrix element between these two states vanishes: a nonzero contribution requires the corresponding T-matrix elements to be non-zero for identical initial and final partial waves. However, symmetric and antisymmetric states correspond to opposite partial-wave parities. Thus, no interference survives in the basis $(|0, 0\rangle, |0, 1\rangle_s, |0, 1\rangle_a, |1, 1\rangle)$. Nevertheless, the relative phase from the original superpositions (1), (2) is not lost but instead manifests as a redistribution of populations in this symmetrized basis [39].

Since the CCS matrix is diagonal, the total cross sec-

tion from the non-entangled superposition becomes:

$$\begin{aligned} \sigma^{ident}(\theta, \beta) = & \cos^4 \theta \sigma_{0,0} + \cos^2 \theta \sin^2 \theta \sigma_{0,1}^s \\ & + \cos^2 \theta \sin^2 \theta \sigma_{0,1}^a + \sin^4 \theta \sigma_{1,1} \quad (6) \\ & + 2 \cos^2 \theta \sin^2 \theta \sigma_{int}(\beta) \end{aligned}$$

where the total interference term $\sigma_{int}(\beta)$ takes the simple form:

$$\sigma_{int}(\beta) = \frac{\sigma_{0,1}^s}{2} \cos(\beta) + \frac{\sigma_{0,1}^a}{2} \cos(\beta + \pi) \quad (7)$$

Coherent control of the total cross section involves four contributions: $\sigma_{0,0}$, $\sigma_{0,1}^s$, $\sigma_{0,1}^a$, and $\sigma_{1,1}$. The two satellite terms are independent of β , while the symmetric and antisymmetric terms vary oppositely with β (maximized at $\beta = 0$ or π , respectively). Coherent control thus arises from the competition between the symmetric and antisymmetric contributions.

In the ultracold regime, scattering is dominated by the s -wave. For identical fermions, only the antisymmetric channel contributes in the s -wave limit:

$$\sigma^{fermion}(\theta, \beta) \approx \frac{\cos^2 \theta \sin^2 \theta}{2} |1 - e^{i\beta}|^2 \sigma_{0,1}^a \quad (8)$$

leading to a perfect control from 0 ($\beta = 0$) to $2 \cos^2 \theta \sin^2 \theta \sigma_{0,1}^a$ ($\beta = \pi$). For identical bosons, the symmetric channel and satellite states contribute via s -wave scattering:

$$\begin{aligned} \sigma^{bosons}(\theta, \beta) \approx & \cos^4 \theta \sigma_{0,0} + \frac{\cos^2 \theta \sin^2 \theta}{2} |1 + e^{i\beta}|^2 \sigma_{0,1}^s \\ & + \sin^4 \theta \sigma_{1,1} \quad (9) \end{aligned}$$

Control remains synchronized, but extrema are reversed ($\beta = 0$ maximum, $\beta = \pi$ minimum) and satellite terms can weaken the control.

The extent of control is quantified by the visibility[16, 39]:

$$\begin{aligned} V(\theta) = & \frac{\sigma_{max}(\theta, \beta_{max}) - \sigma_{min}(\theta, \beta_{min})}{\sigma_{max}(\theta, \beta_{max}) + \sigma_{min}(\theta, \beta_{min})} \\ = & \frac{\left| \frac{\sigma_{0,1}^s}{\sigma_{0,1}^a} - 1 \right|}{\cot^2 \theta \frac{\sigma_{0,0}}{\sigma_{0,1}^a} + \tan^2 \theta \frac{\sigma_{1,1}}{\sigma_{0,1}^a} + \frac{\sigma_{0,1}^s}{\sigma_{0,1}^a} + 1}, \quad (10) \end{aligned}$$

which depends on the ratio of symmetric to antisymmetric contributions, $\sigma_{0,1}^s/\sigma_{0,1}^a$, and the weights of the satellite terms, $\sigma_{0,0}/\sigma_{0,1}^a$ and $\sigma_{1,1}/\sigma_{0,1}^a$. Visibility is high when one contribution dominates (e.g., in the ultracold regime) and vanishes when $\sigma_{0,1}^s \approx \sigma_{0,1}^a$, reflecting the competition between symmetric and antisymmetric contributions.

Comparing Eqs. (4)–(5) for non-identical particles with Eqs. (6)–(7) for identical particles shows that exchange symmetry removes key limitations of coherent control. In the non-identical case, phase shifts vary across final states

and partial waves, leading to partial-wave and internal-state scrambling upon summation. For identical particles, exchange symmetry restricts phases to 0 or π set by scattering parity. In the ultracold regime, a single parity typically dominates, suppressing scrambling and enforcing pathway indistinguishability.

Examples of symmetry-synchronized coherent control with lithium isotopologues in the ultracold regime. To illustrate symmetry-enforced synchronization of coherent control, we perform zero-field coupled-channel calculations for ${}^6\text{Li}+{}^6\text{Li}$ (identical fermions), ${}^7\text{Li}+{}^7\text{Li}$ (identical bosons), and ${}^6\text{Li}+{}^7\text{Li}$ (distinguishable), comparing identical-particle collisions to a heteronuclear case without symmetry-locked phases. We model ground-state alkali-atom collisions as in Ref. [43] and compute multichannel T -matrix elements using MOLSCAT [42] at $T = 20 \mu\text{K}$ unless stated otherwise; further details are in the Supplementary Material [37]. From these, we construct CCS matrix elements (Eq. 3) in unsymmetrized and symmetrized bases for non-identical and identical cases, respectively, and evaluate $\sigma = \mathbf{a}^\dagger \mathbf{C} \mathbf{a}$.

The Li atoms are prepared in the coherent superposition given in equations (1) and (2). To illustrate the control, we use the following representative internal states: $|0\rangle \equiv |f = 1/2, m_f = 1/2\rangle_{6\text{Li}}$ and $|1\rangle \equiv |f = 3/2, m_f = 1/2\rangle_{6\text{Li}}$ for homonuclear ${}^6\text{Li}+{}^6\text{Li}$ collisions, $|0\rangle \equiv |f = 1, m_f = -1\rangle_{7\text{Li}}$ and $|1\rangle \equiv |f = 2, m_f = -2\rangle_{7\text{Li}}$ for homonuclear ${}^7\text{Li}+{}^7\text{Li}$ collisions. For heteronuclear collisions, we choose $|0\rangle_6 \equiv |f = 1/2, m_f = 1/2\rangle_{6\text{Li}}$, $|1\rangle_6 \equiv |f = 1/2, m_f = -1/2\rangle_{6\text{Li}}$, $|0\rangle_7 \equiv |f = 1, m_f = 1\rangle_{7\text{Li}}$, and $|1\rangle_7 \equiv |f = 1, m_f = 0\rangle_{7\text{Li}}$. The final channels populated by collisions between atoms prepared in these superpositions correspond to elastic scattering, spin-exchange processes, or dipolar relaxation into lower hyperfine states. A practical route to prepare these superpositions uses two initially separated atomic ensembles (tweezers or optical traps) that are independently prepared and then merged for collisions. Similar schemes have been proposed for ultracold-molecule interferometry, where site-selective AC Stark shifts and phase-coherent microwave pulses imprint a controllable relative phase before merging [18]. For lithium atoms, rf/microwave fields and differential light shifts can set the control phase β between entrance pathways. The effectiveness of this control is sensitive to any dephasing which may occur between state preparation and collision.

The visibilities for fermionic, bosonic, and non-identical cases are compared in Fig. 2(a). For fermionic ${}^6\text{Li}+{}^6\text{Li}$ collisions, control is near-perfect ($V \simeq 1$), consistent with Eq. (8): symmetry suppresses satellite and symmetric contributions, leaving the antisymmetric channel dominant and producing synchronized control with a minimum at $\beta = 0$ [Fig. 2(b)]. For bosonic ${}^7\text{Li}+{}^7\text{Li}$, control is reduced but still significant ($V = 0.7$) due to satellite contributions, though symmetry still synchronizes the main channel with a shifted minimum near

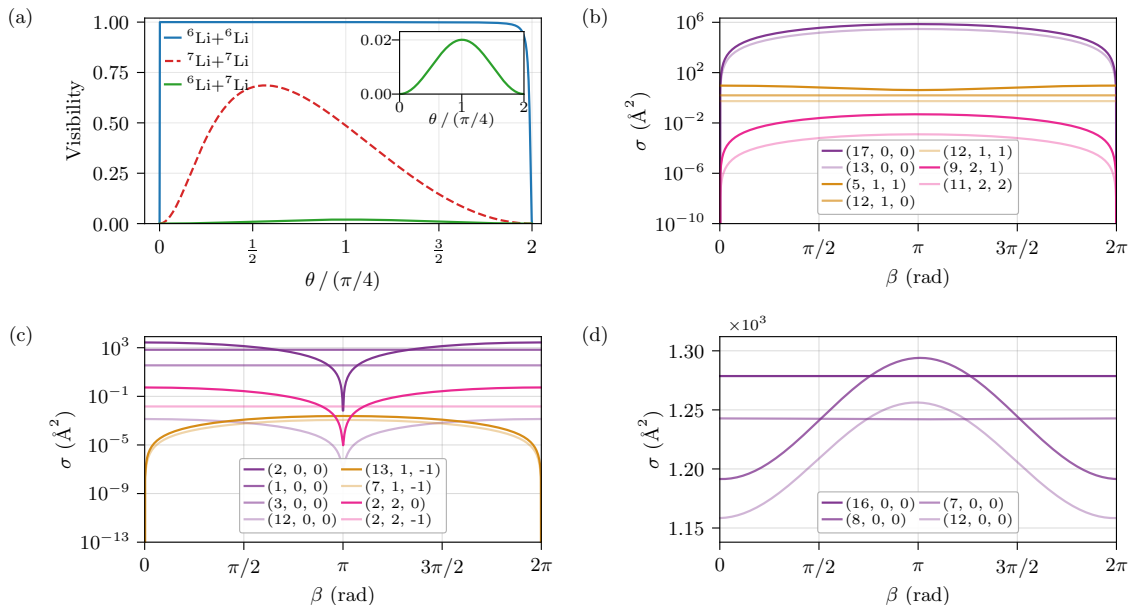


FIG. 2: (a) Visibility V of the total cross-section control versus θ for ${}^6\text{Li}+{}^6\text{Li}$, ${}^7\text{Li}+{}^7\text{Li}$, and ${}^6\text{Li}+{}^7\text{Li}$ at $E = 20\mu\text{K}$; the inset zooms in for ${}^6\text{Li}+{}^7\text{Li}$. (b)–(d): Dominant partial-wave-resolved state-to-state cross sections for (b) ${}^6\text{Li}+{}^6\text{Li}$, (c) ${}^7\text{Li}+{}^7\text{Li}$, and (d) ${}^6\text{Li}+{}^7\text{Li}$. Labels denote exit-channel quantum numbers $(\alpha_{\text{out}}, L_{\text{out}}, m_{L,\text{out}})$, each α_{out} labels one specific combination of internal quantum numbers used in MOLSCAT[42], e.g., $((f_1, m_{f_1}, f_2, m_{f_2}))$ for the collisions between two atoms; colors indicate partial waves and opacity indicates hyperfine exit channels. The flat traces of the state-to-state cross sections are due to satellite terms.

π [Fig. 2(c)]. Entangled initial states can suppress satellite effects and restore near-unity visibility (see Supplementary Material [37]). In contrast, the distinguishable ${}^6\text{Li}+{}^7\text{Li}$ mixture shows very weak control ($V \simeq 0.01$) because pathway indistinguishability cannot be enforced across all channels [37].

Beyond the ultracold regime. As collision energy increases, more partial waves become accessible, but exchange symmetry in identical particles still enforces identical phase shifts within each parity sector. As a result, no partial-wave or hyperfine scrambling occurs within a given parity sector. This is illustrated in Fig. 3(b,c) at 1 K, where contributions are summed over hyperfine states for fixed partial waves: even and odd channels each show synchronized control. Tuning β allows switching between regimes dominated by even or odd partial waves. This parity-selective control is robust with temperature and is a hallmark of coherent control in identical-particle scattering.

The parity switch is possible because contributions from opposite-parity channels are out of phase. On the other hands, when summed, they cancel each other, leading to a reduced visibility of the total cross section [Fig. 3(a)], which vanishes when the contributions from the two parities become equal, and is directly related to the ratio $\sigma_{01}^s/\sigma_{01}^a$ [Eq. (10)]. This condition is reached beyond the p -wave centrifugal barrier (approximately 10

mK), above which s - and p -wave contributions become comparable.

In contrast, heteronuclear cases exhibit both hyperfine and partial-wave scrambling. Hyperfine scrambling reduces control when summing over hyperfine states at fixed partial wave, as shown in Fig. 7 of the Supplementary Material [37]. Partial-wave scrambling, shown in Fig. 3(d), arises within each parity sector from the lack of synchronization: channels such as $L = 1$ and $L = 3$ (and $L = 2$ and $L = 6$) are out of phase. Consequently, tuning β controls neither the parity nor the total cross section in the heteronuclear case.

Discussion and conclusions. We have shown that exchange symmetry of identical collision partners phase-synchronizes the state-to-state cross sections of different exit channels with the same partial wave parity, and leverages this property to theoretically demonstrate strong control of bimolecular collisions. In the ultracold regime, this allows full tuning of the total cross section, while at higher energies it enables controlled manipulation of final-state parity. By overcoming phase scrambling limitations of previous approaches, this work demonstrates coherent control of a total cross section, with control over the parity of the exit channels remaining robust at elevated temperatures.

Symmetry-synchronized control in Li+Li collisions provides a starting point for extending coherent-control

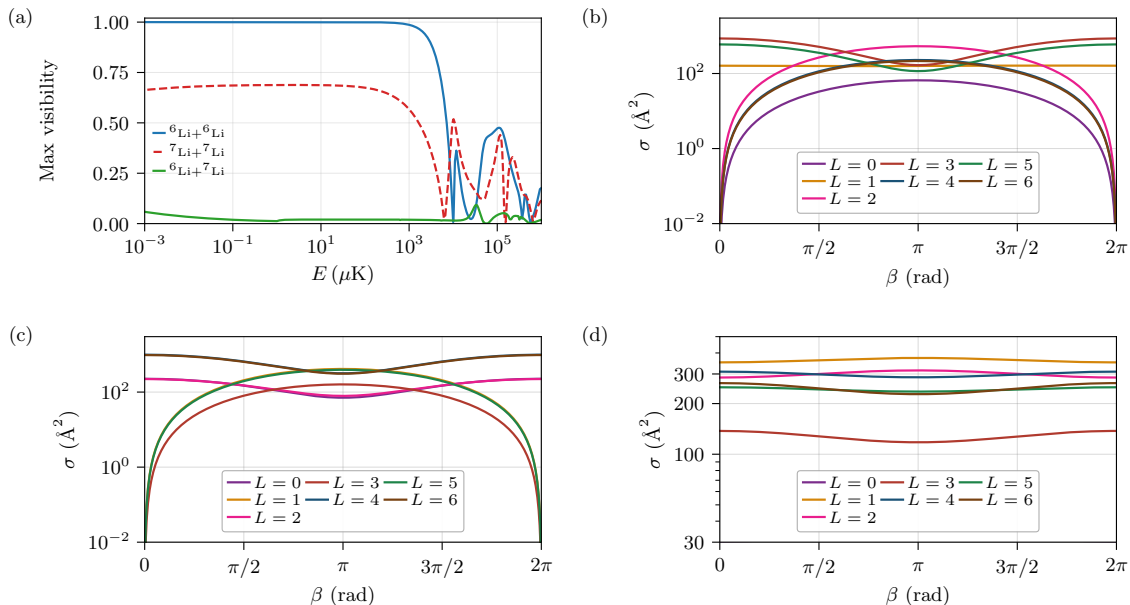


FIG. 3: (a): Maximum visibility V of the total cross-section control versus collision energy E for ${}^6\text{Li}+{}^6\text{Li}$, ${}^7\text{Li}+{}^7\text{Li}$, and ${}^6\text{Li}+{}^7\text{Li}$. (b)–(d): Total cross sections at different partial waves at $E = 1$ K for (b) ${}^6\text{Li}+{}^6\text{Li}$, (c) ${}^7\text{Li}+{}^7\text{Li}$, and (d) ${}^6\text{Li}+{}^7\text{Li}$.

strategies to other molecular systems. Our protocol is particularly useful for homonuclear systems, where collisional control using external electric fields is not applicable because they lack permanent dipole moments, where short-range dynamics are complex and microwave shielding is ineffective. The protocol applies broadly to identical particles and does not lose effectiveness as the number of final states grows, opening new avenues for controlling collisions such as Li_2 – Li_2 and Sr_2 – Sr_2 .

Acknowledgement. We thank the discussions during the quantum control GRC 2025. This work was supported by the U.S. Air Force Office of Scientific Research (AFOSR) under Contract No. FA9550-22-1-0361, Jing-Chen Zhang and Yu Liu are supported by the start up fund at the department of chemistry in the University of Maryland, College Park. Jing-Chen Zhang thanks the valuable discussions with Kang-Kuen Ni and Kaden Hazard.

* iczhang@terpmail.umd.edu
 † adrien.devolder@utoronto.ca
 ‡ ttscherbul@unr.edu
 § paul.brumer@utoronto.ca
 ¶ yuliu@umd.edu

- [1] C. Gross and I. Bloch, Quantum simulations with ultracold atoms in optical lattices, *Science* **357**, 995 (2017).
 [2] S. L. Cornish, M. R. Tarbutt, and K. R. A. Hazzard, Quantum computation and quantum simulation with ultracold molecules, *Nature Physics* **20**, 730 (2024).

- [3] T. Karman, M. Tomza, and J. Pérez-Ríos, Ultracold chemistry as a testbed for few-body physics, *Nature Physics* **20**, 722 (2024).
 [4] L. D. Carr, D. DeMille, R. V. Krems, and J. Ye, Cold and ultracold molecules: science, technology and applications, *New J. Phys.* **11**, 055049 (2009).
 [5] J. L. Bohn, A. M. Rey, and J. Ye, Cold molecules: Progress in quantum engineering of chemistry and quantum matter, *Science* **357**, 1002 (2017).
 [6] C. Chin, R. Grimm, P. Julienne, and E. Tiesinga, Feshbach resonances in ultracold gases, *Rev. Mod. Phys.* **82**, 1225 (2010).
 [7] J. J. Park, Y.-K. Lu, A. O. Jamison, T. V. Tscherbul, and W. Ketterle, A feshbach resonance in collisions between triplet ground-state molecules, *Nature* **614**, 54 (2023).
 [8] Y. Liu and K.-K. Ni, Bimolecular chemistry in the ultracold regime, *Annu. Rev. Phys. Chem.* **73**, 73 (2022).
 [9] T. V. Tscherbul and R. V. Krems, Tuning bimolecular chemical reactions by electric fields, *Phys. Rev. Lett.* **115**, 023201 (2015).
 [10] G. Quémener and P. S. Julienne, Ultracold molecules under control!, *Chemical Reviews* **112**, 4949 (2012).
 [11] K.-K. Ni, S. Ospelkaus, D. Wang, G. Quémener, B. Neyenhuis, M. H. G. de Miranda, J. L. Bohn, D. S. Jin, and J. Ye, Dipolar collisions of polar molecules in the quantum regime, *Nature* **464**, 1324 (2010).
 [12] M.-G. Hu, Y. Liu, D. D. Grimes, Y.-W. Lin, A. H. Gheorghe, R. Vexiau, N. Bouloufa-Maafa, O. Dulieu, T. Rosenband, and K.-K. Ni, Direct observation of bimolecular reactions of ultracold KRb molecules, *Science* **366**, 1111 (2019).
 [13] R. V. Krems, Cold controlled chemistry, *Phys. Chem. Chem. Phys.* **10**, 4079 (2008).

- [14] M. Shapiro and P. Brumer, *Quantum control of Molecular Processes* (Wiley-VCH, 2012).
- [15] J. Gong, M. Shapiro, and P. Brumer, Entanglement-assisted coherent control in nonreactive diatom–diatom scattering, *J. Chem. Phys.* **118**, 2626 (2003).
- [16] A. Devolder, T. V. Tscherbul, and P. Brumer, Robust coherent control of two-body collisions beyond the ultracold regime, *Phys. Rev. Research* **5**, L042025 (2023).
- [17] A. Devolder, T. V. Tscherbul, and P. Brumer, Leveraging reactant entanglement in the coherent control of ultracold bimolecular chemical reactions, *Phys. Rev. Lett.* **135**, 233401 (2025).
- [18] J. Luke, L. Zhu, Y.-X. Liu, and K.-K. Ni, Reaction interferometry with ultracold molecules, *Faraday Discuss.* **251**, 63 (2024).
- [19] Y.-X. Liu, L. Zhu, J. Luke, J. J. A. Houwman, M. C. Babin, M.-G. Hu, and K.-K. Ni, Quantum interference in atom-exchange reactions, *Science* **384**, 1117 (2024).
- [20] A. Devolder, T. V. Tscherbul, and P. Brumer, Time-reversal symmetry-protected coherent control of ultracold molecular collisions, *J. Phys. Chem. Lett.* **16**, 2808 (2025).
- [21] T. Karman and J. M. Hutson, Microwave shielding of ultracold polar molecules, *Phys. Rev. Lett.* **121**, 163401 (2018).
- [22] L. Lassabliere and G. Quemener, Controlling the scattering length of ultracold dipolar molecules, *Phys. Rev. Lett.* **121**, 163402 (2018).
- [23] L. Anderegg, S. Burchesky, Y. Bao, S. Yu, T. Karman, E. Chae, K.-K. Ni, W. Ketterle, and J. M. Doyle, Observation of microwave shielding of ultracold molecules, *Science* **373**, 779 (2021).
- [24] N. Bigagli, W. Yuan, S. Zhang, B. Bulatovic, T. Karman, I. Stevenson, and S. Will, Observation of Bose–Einstein condensation of dipolar molecules, *Nature* **631**, 289 (2024).
- [25] T. Karman, N. Bigagli, W. Yuan, S. Zhang, I. Stevenson, and S. Will, Double microwave shielding, *PRX Quantum* **6**, 020358 (2025).
- [26] Z. Shi, Z. Huang, F. Deng, W.-J. Jin, S. Yi, T. Shi, and D. Wang, Bose-einstein condensate of ultracold sodium-rubidium molecules with tunable dipolar interactions (2025), [arXiv:2508.20518 \[cond-mat.quant-gas\]](https://arxiv.org/abs/2508.20518).
- [27] Y.-X. Liu, L. Zhu, J. Luke, M. C. Babin, M. Gronowski, H. Ladjimi, M. Tomza, J. L. Bohn, T. V. Tscherbul, and K.-K. Ni, Hyperfine-to-rotational energy transfer in ultracold atom–molecule collisions of Rb and KRb, *Nature Chemistry* **17**, 688 (2025).
- [28] P. Wurtz, T. Gericke, A. Vogler, and H. Ott, Ultracold atoms as a target: absolute scattering cross-section measurements, *New J. Phys.* **12**, 065033 (2010).
- [29] A. P. P. van der Poel and H. L. Bethlem, A detailed account of the measurements of cold collisions in a molecular synchrotron, *EPJ Techniques and Instrumentation* **5**, 6 (2018).
- [30] A. Devolder, T. V. Tscherbul, and P. Brumer, Coherent multichannel optical theorem: Quantum control of the total scattering cross section, *Phys. Rev. A* **105**, 052808 (2022).
- [31] A. Devolder, T. V. Tscherbul, and P. Brumer, Coherent control of ultracold molecular collisions: The role of resonances, *The Journal of Physical Chemistry Letters* **14**, 2171 (2023).
- [32] P. Brumer, K. Bergmann, and M. Shapiro, Identical collision partners in the coherent control of bimolecular reactions, *J. Chem. Phys.* **113**, 2053 (2000).
- [33] P. Brumer, A. Abrashkevich, and M. Shapiro, Laboratory conditions in the coherent control of reactive scattering, *Faraday Discussion* **113**, 291 (1999).
- [34] Y. Bao, S. S. Yu, L. Anderegg, E. Chae, W. Ketterle, K.-K. Ni, and J. M. Doyle, Dipolar spin-exchange and entanglement between molecules in an optical tweezer array, *Science* **382**, 1138 (2023).
- [35] L. R. B. Picard, A. J. Park, G. E. Patenotte, S. Gebretsadkan, D. Wellnitz, A. M. Rey, and K.-K. Ni, Entanglement and iSWAP gate between molecular qubits, *Nature* **637**, 821 (2025).
- [36] D. K. Ruttley, T. R. Hepworth, A. Guttridge, and S. L. Cornish, Long-lived entanglement of molecules in magic-wavelength optical tweezers, *Nature* **637**, 827 (2025).
- [37] See Supplemental Material at [URL will be inserted by publisher] for details of the coupled-channel calculations and interaction potentials, the general coherent control scattering matrix formalism, coherent control in the unsymmetrized basis, quantification of parity control, a comparison of product versus entangled initial-state preparations, and the behavior of state-to-state cross sections at higher collision energies.
- [38] E. Frishman, M. Shapiro, and P. Brumer, Optimized imploding waves in the coherent control of bimolecular processes: Atom-rotor scattering, *J. Phys. Chem. A* **103**, 10333 (1999).
- [39] A. Devolder, T. V. Tscherbul, and P. Brumer, Interference is in the eye of the beholder: Application to the coherent control of collisional processes, *The Journal of Chemical Physics* **160**, 174304 (2024).
- [40] J. J. Omiste, J. Floß, and P. Brumer, Coherent control of penning and associative ionization: Insights from symmetries, *Phys. Rev. Lett.* **121**, 163405 (2018).
- [41] A. Devolder, P. Brumer, and T. V. Tscherbul, Complete quantum coherent control of ultracold molecular collisions, *Phys. Rev. Lett.* **126**, 153403 (2021).
- [42] J. M. Hutson and C. R. Le Sueur, MOLSCAT: A program for non-reactive quantum scattering calculations on atomic and molecular collisions, *Computer Physics Communications* **241**, 9–18 (2019).
- [43] J.-C. Zhang, P. Julienne, and Y. Liu, Characterization of feshbach resonances in a ${}^6\text{Li}$ – ${}^7\text{Li}$ mixture using improved interaction potentials, *Phys. Rev. A* **113**, 062802 (2026).

Supplemental Material: Identical-Particle Symmetry-Enabled Complete Coherent Control of Ultracold Atomic and Molecular Collisions

Jing-Chen Zhang(张京晨),^{1,2,3} Adrien Devolder,⁴ Timur V. Tscherbul,⁵ Paul Brumer,⁴ and Yu Liu^{1,2,3}

¹*Institute for Physical Science and Technology, University of Maryland, College Park, Maryland 20742, USA*

²*Department of Chemistry and Chemical Biology,*

University of Maryland, College Park, Maryland 20742, USA

³*Joint Quantum Institute, University of Maryland and National Institute of Standards and Technology (NIST), College Park, Maryland 20742, USA*

⁴*Chemical Physics Theory Group, Department of Chemistry, and Center for Quantum Information and Quantum Control, University of Toronto, Toronto, Ontario M5S 3H6, Canada*

⁵*Department of Physics, University of Nevada, Reno, Nevada 89557, USA*

OVERVIEW

This Supplemental Material provides additional technical details and supporting results organized around the following topics:

1. **Details of coupled-channel calculations:** The Hamiltonian, interaction potentials, together with the mapping of asymptotic hyperfine states onto the coherent-control qubit manifold, and a discussion of alternative channel choices and magnetic field effect.
2. **General introduction of coherent control of collisions**
3. **General coherent control scattering matrix formalism** General introduction of the coherent control scattering matrix formalism [S1, S2]
4. **Coherent control of identical particle collisions in unsymmetrized basis**
5. **Initial-state preparation: product versus entangled superpositions:** A comparison of coherent control using entangled superpositions versus product-state preparation, highlighting how the former removes satellite terms and enhances the visibility of the total scattering cross section.
6. **Identical particle case with different states in the superposition of the two molecules** Demonstration that if different internal states are used in the initial coherent superposition, synchronization is lost.
7. **Behaviors of partial state-to-state cross sections at higher collision energies:** An explicit demonstration showing that, for identical particles, state-to-state contributions across different partial waves exhibit synchronization even at higher collisional energies beyond ultracold regime, and how this synchronization disappears for heteronuclear systems.

1. DETAILS OF COUPLED-CHANNEL CALCULATIONS

Hamiltonian and interaction potentials

The Hamiltonian describing the relative motion of two Li atoms in their electronic ground state is

$$\hat{H} = -\frac{\hbar^2}{2\mu} \frac{1}{R} \frac{d^2}{dR^2} R + \frac{\hat{L}^2}{2\mu R^2} + \hat{h}_a + \hat{h}_b + \hat{V}(R), \quad (\text{S1})$$

where μ is the reduced mass, R is the internuclear separation, and \hat{L} is the relative orbital angular momentum operator. The single-atom Hamiltonians \hat{h}_j for $j \in \{a, b\}$ include hyperfine and Zeeman interactions,

$$\hat{h}_j = \zeta_j \hat{\mathbf{I}}_j \cdot \hat{\mathbf{s}}_j + (g_e \mu_B \hat{s}_{zj} + g_{i,j} \mu_N \hat{I}_{zj}) B, \quad (\text{S2})$$

where ζ_j is the hyperfine constant and g_e and $g_{i,j}$ are the electron and nuclear g -factors.

The interaction potential $\hat{V}(R)$ includes the isotropic adiabatic electronic potentials and the anisotropic magnetic dipole-dipole interaction $\hat{V}^d(R)$:

$$\hat{V}(R) = V_0(R) \hat{P}_0 + V_1(R) \hat{P}_1 + \hat{V}^d(R) + \sum_{S=0,1} V_{\text{shift},S}(R). \quad (\text{S3})$$

Here, $\hat{P}_{0(1)}$ projects onto the electronic singlet $S = 0$ (triplet $S = 1$) subspace. The dipole term $\hat{V}^d(R)$, dominated by spin-spin coupling, induces weak anisotropic couplings with $\Delta L = \pm 2$ and is given by:

$$\hat{V}^d(R) = \frac{E_h \alpha^2}{(R/a_0)^3} [\hat{s}_a \cdot \hat{s}_b - 3(\hat{s}_a \cdot \mathbf{e}_R)(\hat{s}_b \cdot \mathbf{e}_R)]. \quad (\text{S4})$$

We represent the singlet ($X^1\Sigma^+$) and triplet ($a^3\Sigma^+$) Li₂ potentials using spectroscopically fitted Morse/Long-Range (MLR) potentials [S3, S4] with correction terms [S5]:

$$V_{\text{MLR}}(R) = D_e \left[1 - \frac{u_{\text{LR}}(R)}{u_{\text{LR}}(R_e)} e^{-\beta(R) y_p(R)} \right]^2, \quad (\text{S5})$$

where D_e is the dissociation energy, u_{LR} enforces the correct long-range van der Waals behavior, and the polynomial $\beta(R)$ controls the short-range shape.

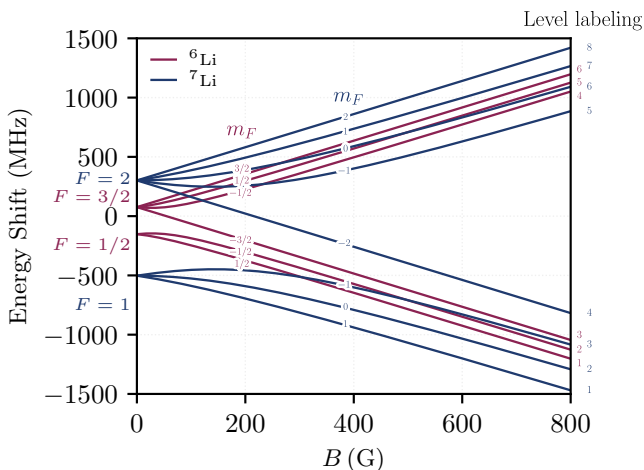


FIG. S1: Zeeman shifts of the hyperfine levels in the electronic ground state ($^2S_{1/2}$) of ^6Li (red) and ^7Li (blue), labeled by the corresponding quantum numbers f and m_f . The zero of energy is defined as the energy in the absence of hyperfine and Zeeman interactions. The numbers on the right label the atomic hyperfine states used to specify each atom in a scattering channel at non-zero B .

We apply a quadratic correction term to the inner wall ($R < R_{e,s}$) of the adiabatic potentials:

$$V_{\text{shift},S}(R) = \mathcal{S}_S (R - R_{e,S})^2. \quad (\text{S6})$$

The shift parameter \mathcal{S}_S enables fine tuning of scattering lengths and Feshbach resonance locations. Details of the potential parameters, including the shift terms, can be found in Ref. [S5].

We solve the coupled-channel equations using MOLSCAT [S6]. The total Hamiltonian is block-diagonal in total angular momentum projection M_{tot} and parity $(-1)^L$. We use propagator method to solve the scattering wavefunctions in each symmetry sector. The propagation uses the hybrid log-derivative/Airy method from the inner wall to long range. In the short-range region we use a fixed radial step size $dr = 0.002 a_0$, while the Airy propagator employs its standard adaptive step-size control at long range. We propagate from $R = 1.8 a_0$ to $R = 3 \times 10^5 a_0$, and the numerical convergence was verified against variations of the propagator parameters. We used $L_{\text{max}} = 2$ between $E = 0.5 \text{ nK}$ and $E = 1 \mu\text{K}$ for ultracold regime and $L_{\text{max}} = 6$ for calculations at higher collision energies, between $1 \mu\text{K}$ and 1 K , to ensure the accurate description of shape resonances of $\text{Li} + \text{Li}$ at high collision energies.

Channel ordering and mapping to hyperfine labels

For the convenience of discussion in the supplementary material, we label the scattering channels by the adia-

batic hyperfine states of Li atoms at $B > 0$, as shown in Fig. S1. The asymptotic states are ordered by increasing threshold energies at $B = 0.1 \text{ G}$ (the magnetic field value used for all scattering calculations throughout the paper, unless stated otherwise). We thus define a two-level qubit manifold $\{|0\rangle, |1\rangle\}$ for each collision case ($^6\text{Li} + ^6\text{Li}$, $^7\text{Li} + ^7\text{Li}$, and $^6\text{Li} + ^7\text{Li}$) by mapping the specific states used for coherent control to these adiabatic hyperfine states, as summarized in Table S1.

Specific hyperfine states were selected to illustrate how control behavior varies across isotopologues. For the homonuclear systems ($^6\text{Li} + ^6\text{Li}$ and $^7\text{Li} + ^7\text{Li}$), we chose scattering channels that exhibit strong inelastic relaxation to other adiabatic hyperfine channels; this often complicates magnetic-field tuning and presumably degrades control by increasing the number of populated channels. Conversely, for the heteronuclear $^6\text{Li} + ^7\text{Li}$ system, channels were chosen for their simpler bound-state spectrum in a magnetic field, which facilitates better control. We emphasize, however, that weaker coupling to open channels does not intrinsically guarantee higher visibility in the total scattering cross section. Although we have the freedom to choose other entrance channels, the conclusions regarding identical particle symmetry presented here are general and independent of the specific entrance channel selected.

To demonstrate that the coherent-control mechanism is not limited to the specific entrance channels used in the main text, we examined alternative choices for the entrance channels. Figures S2 displays the maximum visibility for representative channel selections in $^6\text{Li} + ^6\text{Li}$, $^7\text{Li} + ^7\text{Li}$, and $^6\text{Li} + ^7\text{Li}$. Although the absolute visibility is channel-dependent—with particularly large low-energy visibility for certain $^6\text{Li} + ^7\text{Li}$ combinations and the $^7\text{Li} + ^7\text{Li}$ pair (3,8)—the underlying mechanism of identical particle symmetry is general and applies to arbitrary initial channel combinations.

TABLE S1: The two-level manifold $\{|0\rangle, |1\rangle\}$ used for coherent control, specified by the single-atom approximate hyperfine quantum numbers $|F, m_F\rangle$ at $B = 0.1 \text{ G}$; see Fig. S1 for the reference to the asymptotic channel numbers at different B .

System	Label	$^6\text{Li} (F, m_F\rangle)$	$^7\text{Li} (F, m_F\rangle)$
$^6\text{Li} - ^6\text{Li}$	$ 0\rangle$	$ \frac{1}{2}, \frac{1}{2}\rangle$	—
	$ 1\rangle$	$ \frac{3}{2}, +\frac{1}{2}\rangle$	—
$^7\text{Li} - ^7\text{Li}$	$ 0\rangle$	—	$ 1, +1\rangle$
	$ 1\rangle$	—	$ 2, -2\rangle$
$^6\text{Li} - ^7\text{Li}$	$ 0\rangle$	$ \frac{1}{2}, \frac{1}{2}\rangle$	$ 1, -1\rangle$
	$ 1\rangle$	$ \frac{3}{2}, +\frac{1}{2}\rangle$	$ 1, 0\rangle$

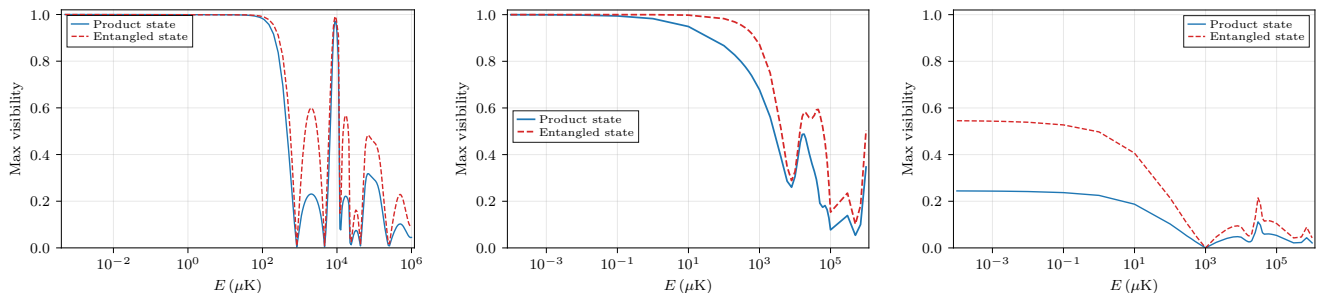


FIG. S2: Energy dependence of the maximum visibility for alternative initial channel pairs. (a) ${}^6\text{Li}$ - ${}^6\text{Li}$ collisions prepared in channel pair (1, 2) at $B = 3$ G. This channel exhibits strong resonance structure at low field (0.1 G) in the ultracold regime ($E < 1$ μK); the higher field is chosen to avoid unwanted resonances. (b) ${}^7\text{Li}$ - ${}^7\text{Li}$ collisions prepared in channel pair (3, 8) at $B = 0.1$ G. (c) ${}^6\text{Li}$ - ${}^7\text{Li}$ collisions for channel pair (2, 6)–(1, 7) (see Fig. S1) at $B = 0.1$ G; curves correspond to the diagonal and off-diagonal blocks of the two-channel scattering problem.

Shape resonances in Li+Li collisions beyond the ultracold regime

In Li+Li collisions, shape resonances arise when a quasi-bound state supported by the centrifugal barrier couples to the scattering continuum within the same partial wave. For instance, the p -wave ($L = 1$) shape resonance occurs at ~ 10 mK. Within the coherent-control protocol, these resonances manifest as enhanced maximum visibility and rapid variations in scattering phase near the resonance energy (see Fig. 3 of the main text and Figs. S3(a) for ${}^6\text{Li}+{}^6\text{Li}$).

Similarly, we can examine this for ${}^7\text{Li}+{}^7\text{Li}$ and ${}^6\text{Li}+{}^7\text{Li}$ collisions, as shown in Figs. S3(b) and Figs. S3(c), respectively. The shape resonances are clearly visible in the partial-wave-resolved state-to-state cross sections, and their locations are consistent with the energy dependence of the maximum visibility shown in Figure 3(a) in the main text.

Effects of magnetic field on coherent control in Li+Li collisions

In coherent control, the magnetic field B can serve as an external tuning parameter that can modify both the magnitudes and phases of the state-to-state scattering cross sections $\sigma_{ij}(B, E)$, thereby affecting the control of the total scattering cross section for a prepared entrance superposition. Previous studies indicate that isolated resonances can enhance control, whereas overlapping resonances often suppress it [S7].

Our coupled-channel calculations for Li+Li show that magnetic Feshbach resonances can significantly affect the achievable visibility at different E . A systematic characterization of the full (B, E) dependence—including resonance-induced phase winding and multichannel coupling effects—is beyond the scope of this Supplemental

Material and thus deferred to another manuscript. Unless stated otherwise, we therefore focus on the near-zero-field regime ($B = 0.1$ G) or the regime far from Feshbach resonances.

2. GENERAL INTRODUCTION OF COHERENT CONTROL OF COLLISIONS

Coherent control of molecular collisions relies on the preparation of initial states as coherent superpositions of internal molecular degrees of freedom[S8]. In general, such a state can be expressed as

$$|\Psi_{\text{ini}}\rangle = \sum_{i_A=1}^{N_{i_A}} \sum_{i_B=1}^{N_{i_B}} a_{i_A, i_B} |i_A, i_B\rangle, \quad (\text{S7})$$

where $a_{i_A, i_B} \in \mathbb{C}$ are complex probability amplitudes satisfying the normalization condition $\sum_{i_A, i_B} |a_{i_A, i_B}|^2 = 1$. The internal states $|i_A\rangle$ and $|i_B\rangle$ may correspond to vibrational, rotational, spin, or other relevant degrees of freedom, depending on the physical system under consideration. This expression represents the most general pure state in the product Hilbert space $\mathcal{H}_{\text{int}}, A \otimes \mathcal{H}_{\text{int}}, B$, and it may exhibit quantum entanglement between the two subsystems.

Such coherent superpositions give rise to multiple indistinguishable scattering pathways whose associated amplitudes interfere. The resulting interference pattern depends sensitively on the relative phases of the coefficients a_{i_A, i_B} , which are determined by the state preparation. Consequently, controlled manipulation of these relative phases enables the modulation of interference effects, providing a mechanism to tune and control observable quantities in the scattering process. It is important to emphasize that the occurrence of interference effects is constrained by the symmetry properties of the collision process. In particular, interference between different pathways is only possible when specific selection rules are

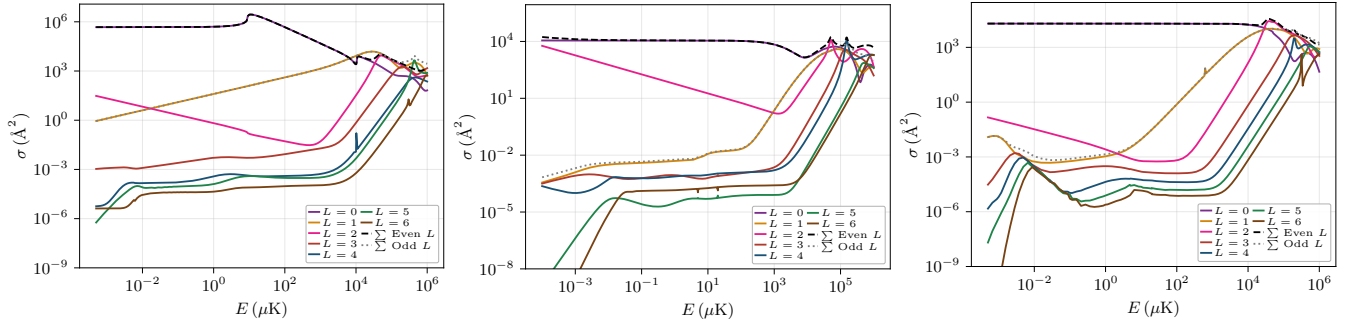


FIG. S3: The total σ per L for different collision cases. (a) ${}^6\text{Li}-{}^6\text{Li}$, (b) ${}^7\text{Li}-{}^7\text{Li}$, (c) ${}^6\text{Li}-{}^7\text{Li}$, Shape resonances are observed for different isotopologues

satisfied. Over time, the following conditions have been identified as necessary for two contributing states to interfere [S8]: (a) they must be energetically degenerate, (b) they must satisfy the same total momentum conservation conditions, and (c) they must share the same projection of the total internal angular momentum onto the quantization axis.

As a representative example, consider an initial state prepared as a coherent superposition of two product states,

$$|\Psi_{\text{ini}}\rangle = \cos \eta, |0\rangle_A |1\rangle_B + \sin \eta, e^{i\beta} |1\rangle_A |0\rangle_B. \quad (\text{S8})$$

The state-to-state integral cross section from this superposition to a given final state f can be written as

$$\begin{aligned} \sigma_{\text{sup} \rightarrow f} &= \cos^2 \eta, \sigma_{01 \rightarrow f} + \sin^2 \eta, \sigma_{10 \rightarrow f} \\ &+ 2 \cos \eta \sin \eta, |\sigma_{\text{int}, f}| \cos(\beta - \Phi_f), \end{aligned} \quad (\text{S9})$$

where the interference contribution is defined as

$$\sigma_{\text{int}, f} = \frac{\pi}{k^2} \sum_{\ell, m} \sum_{\ell', m'} T_{0,1,\ell, m \rightarrow f, \ell', m'}, T_{1,0,\ell, m \rightarrow f, \ell', m'}^* \quad (\text{S10})$$

and $\Phi_f = \arg(\sigma_{\text{int}, f})$ denotes its phase.

The cross section exhibits a harmonic dependence on the relative phase β , which provides the basis for coherent control. The degree of control is determined by the relative magnitude of the interference term compared to the incoherent contributions (the first two terms). To quantify this effect, one introduces the visibility,

$$\begin{aligned} V &= \frac{\sigma_{\text{max}} - \sigma_{\text{min}}}{\sigma_{\text{max}} + \sigma_{\text{min}}} \\ &= \frac{2 \cos \eta \sin \eta |\sigma_{\text{int}, f}|}{\cos^2 \eta \sigma_{01 \rightarrow f} + \sin^2 \eta \sigma_{10 \rightarrow f}}. \end{aligned} \quad (\text{S11})$$

It has been shown that the maximum achievable visibility is given by the ratio

$$R_c = \frac{|\sigma_{\text{int}, f}|}{\sqrt{\sigma_{01 \rightarrow f}, \sigma_{10 \rightarrow f}}}, \quad (\text{S12})$$

referred to as the control index. By construction, $0 \leq R_c \leq 1$. The upper bound $R_c = 1$ is reached when the two pathways are fully indistinguishable, corresponding to equal incoherent contributions. This condition can be expressed as $P(\eta_{\text{max}}) = \frac{|\cos^2 \eta_{\text{max}, \sigma_{01 \rightarrow f}} - \sin^2 \eta_{\text{max}, \sigma_{10 \rightarrow f}}|}{\cos^2 \eta_{\text{max}, \sigma_{01 \rightarrow f}} + \sin^2 \eta_{\text{max}, \sigma_{10 \rightarrow f}}} = 0$

Achieving large values of R_c requires the interference term to approach the geometric mean of the individual cross sections. This condition is closely related to the structure of the control landscape at the level of individual partial-wave transitions. When the interference contributions from all initial-final partial-wave channels add constructively (i.e., are phase-aligned), the control index approaches unity. Conversely, when these contributions are out of phase, destructive competition between channels suppresses the overall interference, leading to reduced controllability and smaller values of R_c . This is called the partial wave scrambling.

3. GENERAL COHERENT CONTROL SCATTERING MATRIX FORMALISM [S1, S2]

First, consider the situation in which the two molecules are prepared in a well-defined initial internal state $|\Psi_{\text{ini}}\rangle = |i_A, i_B\rangle$ where $|i_A\rangle$ and $|i_B\rangle$ denote the internal quantum states of molecules A and B, respectively. Within the standard quantum scattering formalism, the total cross section is obtained from the corresponding T-matrix elements, $T_{i_A, i_B, \ell, m \rightarrow f_1, f_2, \ell', m'}$, as:

$$\sigma = \frac{\pi}{k^2} \sum_{f_1, f_2} \sum_{\ell, m} \sum_{\ell', m'} |T_{i_A, i_B, \ell, m \rightarrow f_1, f_2, \ell', m'}|^2 \quad (\text{S13})$$

where $|f_1\rangle$ is an internal state of the first molecule and $|f_2\rangle$ is an internal state of the second molecule after the collision.

Now, consider the preparation of the two molecules in a general coherent superposition of internal states Eq. S7. For such an initial state, the total cross section is obtained by coherently summing over all contributing scat-

tering amplitudes:

$$\sigma = \frac{\pi}{k^2} \sum_{f_1, f_2} \sum_{\ell, m_\ell} \sum_{\ell' m'_\ell} \left| \sum_{i_A, i_B} a_{i_A, j_B} T_{i_A, i_B, \ell, m_\ell \rightarrow f_1, f_2, \ell', m'_\ell} \right|^2 \quad (\text{S14})$$

Expanding the modulus squared yields a quadratic form in the preparation amplitudes:

$$\begin{aligned} \sigma = & \frac{\pi}{k^2} \sum_{i_A, i_B} \sum_{j_A, j_B} a_{i_A, i_B}^* \\ & \left(\sum_{f_1, f_2} \sum_{\ell, m_\ell} \sum_{\ell' m'_\ell} T_{i_A, i_B, \ell, m_\ell \rightarrow f_1, f_2, \ell', m'_\ell} \right. \\ & \left. \times T_{j_A, j_B, \ell, m_\ell \rightarrow f_1, f_2, \ell', m'_\ell}^* \right) \\ & a_{j_A, j_B} \end{aligned} \quad (\text{S15})$$

We now reinterpret the T -matrix as a rectangular matrix whose rows are indexed by the initial internal states (i_A, i_B) and whose columns collect all remaining quantum numbers ($\ell, m_\ell, f_1, f_2, \ell', m'_\ell$). With this identification, the quantity inside parentheses corresponds to the matrix product $\mathbf{T}\mathbf{T}^\dagger$. This defines the Coherent Control Scattering (CCS) matrix, $\mathbf{C} = \mathbf{T}\mathbf{T}^\dagger$, which acts on the space of initial internal states and has dimension $(N_{i_A} N_{i_B}) \times (N_{j_A} N_{j_B})$. Its matrix elements are explicitly given by [S2]:

$$\begin{aligned} \mathbf{C}_{i_A, i_B; j_A, j_B} = & \sum_{\ell, m_\ell} \sum_{f_1, f_2} \sum_{\ell' m'_\ell} T_{i_A, i_B; \ell, m_\ell, f_1, f_2, \ell', m'_\ell} \\ & \times T_{j_A, j_B; \ell, m_\ell, f_1, f_2, \ell', m'_\ell}^* \end{aligned} \quad (\text{S16})$$

This formulation makes explicit that the control of the cross section through coherent superpositions is governed by the Hermitian, positive semi-definite CCS matrix \mathbf{C} :

$$\sigma = \mathbf{a}^\dagger \mathbf{C} \mathbf{a} \quad (\text{S17})$$

where \mathbf{a} is the vector of the coefficients.

4. COHERENT CONTROL OF IDENTICAL PARTICLE COLLISION IN UNSYMMETRIZED BASIS

In the main text, we developed a formalism describing coherent control of collisions between identical particles using a basis adapted to exchange symmetry. This symmetrized representation naturally separates the dynamics into distinct symmetry sectors and provides a convenient framework to construct the coherent control scattering (CCS) matrix governing the total cross section. In this basis, the CCS matrix takes the diagonal form:

$$\mathbf{C} = \begin{pmatrix} \sigma_{0,0} & 0 & 0 & 0 \\ 0 & \sigma_{0,1}^s & 0 & 0 \\ 0 & 0 & \sigma_{0,1}^a & 0 \\ 0 & 0 & 0 & \sigma_{1,1} \end{pmatrix} \quad (\text{S18})$$

The CCS matrix can be decomposed into contributions from even- and odd-parity components,

$$\mathbf{C} = \begin{pmatrix} \sigma_{0,0} & 0 & 0 & 0 \\ 0 & \sigma_{0,1}^s & 0 & 0 \\ 0 & 0 & 0 & 0 \\ 0 & 0 & 0 & \sigma_{1,1} \end{pmatrix} + \begin{pmatrix} 0 & 0 & 0 & 0 \\ 0 & 0 & 0 & 0 \\ 0 & 0 & \sigma_{0,1}^a & 0 \\ 0 & 0 & 0 & 0 \end{pmatrix} \quad (\text{S19})$$

As shown in the main text, in the symmetrized basis, the CCS matrix is diagonal, reflecting the fact that states belonging to different exchange-symmetry sectors do not interfere. Consequently, no coherent interference terms arise between distinct symmetry-adapted components of the initial state. While this structure simplifies the analysis of identical-particle scattering, it obscures the interpretation of coherent control in terms of interference and complicates a direct comparison with the case of distinguishable particles.

To facilitate this comparison, we transform back to the unsymmetrized basis using the unitary transformation:

$$\mathbf{U} = \begin{pmatrix} 1 & 0 & 0 & 0 \\ 0 & \frac{1}{\sqrt{2}} & \frac{1}{\sqrt{2}} & 0 \\ 0 & \frac{1}{\sqrt{2}} & -\frac{1}{\sqrt{2}} & 0 \\ 0 & 0 & 0 & 1 \end{pmatrix} \quad (\text{S20})$$

The state amplitudes and the CCS matrix transform according to:

$$\mathbf{a}' = \mathbf{U} \mathbf{a} \quad (\text{S21})$$

$$\mathbf{C}' = \mathbf{U} \mathbf{C} \mathbf{U}^\dagger \quad (\text{S22})$$

Applying this transformation to the even- and odd-parity contributions separately yields

$$\mathbf{C}' = \begin{pmatrix} \sigma_{0,0} & 0 & 0 & 0 \\ 0 & \frac{\sigma_{0,1}^s}{2} & \frac{\sigma_{0,1}^s}{2} & 0 \\ 0 & \frac{\sigma_{0,1}^s}{2} & \frac{\sigma_{0,1}^s}{2} & 0 \\ 0 & 0 & 0 & \sigma_{1,1} \end{pmatrix} + \begin{pmatrix} 0 & 0 & 0 & 0 \\ 0 & \frac{\sigma_{0,1}^a}{2} & -\frac{\sigma_{0,1}^a}{2} & 0 \\ 0 & -\frac{\sigma_{0,1}^a}{2} & \frac{\sigma_{0,1}^a}{2} & 0 \\ 0 & 0 & 0 & 0 \end{pmatrix} \quad (\text{S23})$$

Each contribution individually satisfies the Cauchy-Schwarz equality, $|C'_{23}| = \sqrt{C'_{22} C'_{33}}$, indicating maximum interference within each symmetry sector. The two contributions correspond to distinct relative phase shifts between the interfering pathways: one with phase 0 ($e^{i0} = +1$) and the other with phase π ($e^{i\pi} = -1$) see the sign of the interfering term C'_{23} . Moreover, for both contributions individually one finds $C'_{22} = C'_{33}$, reflecting that the two paths are indistinguishable at the level of the transformed basis. Therefore, control is not limited by partial distinguishability between pathways.

Summing the even- and odd-parity contributions yields

$$\mathbf{C}' = \begin{pmatrix} \sigma_{0,0} & 0 & 0 & 0 \\ 0 & \frac{\sigma_{0,1}^s + \sigma_{0,1}^a}{2} & \frac{\sigma_{0,1}^s - \sigma_{0,1}^a}{2} & 0 \\ 0 & \frac{\sigma_{0,1}^s - \sigma_{0,1}^a}{2} & \frac{\sigma_{0,1}^s + \sigma_{0,1}^a}{2} & 0 \\ 0 & 0 & 0 & \sigma_{1,1} \end{pmatrix} \quad (\text{S24})$$

In that case, the competition between the two contributions from the two symmetry sectors reduces the controllability. The Cauchy-Swartz equality is not anymore satisfied: $|C'_{23}| = \frac{|\sigma_{0,1}^s - \sigma_{0,1}^a|}{2} < \sqrt{C'_{22}C'_{33}} = \frac{\sigma_{0,1}^s + \sigma_{0,1}^a}{2}$. Complete coherent control is recovered in regimes where either the even- or odd-parity channel is dominant, such as in the ultracold limit where a single partial-wave contribution typically prevails.

5. INITIAL-STATE PREPARATION: PRODUCT VERSUS ENTANGLED SUPERPOSITIONS

In addition to the product-state superposition

$$|\Psi_{\text{ini}}\rangle = \left(\cos \frac{\theta}{2} |0\rangle + e^{i\beta} \sin \frac{\theta}{2} |1\rangle \right)_a \otimes \left(\cos \frac{\theta}{2} |0\rangle + e^{i\beta} \sin \frac{\theta}{2} |1\rangle \right)_b \quad (\text{S25})$$

analyzed in the main text, one can prepare entangled states that populate exclusively the symmetric and anti-symmetric combinations in the symmetrized basis:

$$\Psi_{\text{ini}} = \frac{\cos \theta + \sin \theta e^{i\beta}}{\sqrt{2}} |0,1\rangle_s + \frac{\cos \theta - \sin \theta e^{i\beta}}{\sqrt{2}} |0,1\rangle_a \quad (\text{S26})$$

where the specific states 0 and 1 used in the paper are defined in Table S1.

These entangled initial states will remove the satellite terms from the total scattering cross sections[S9] and are expected to enhance the visibility across different collisional energies. However, the experimental preparation of entangled initial state is significantly more challenging than that of the product states defined in Eq. (S25).

For the case of non-identical particles, the total cross section can be expressed as:

$$\sigma^{\text{non-ident}}(\theta, \beta) = \cos^2 \theta \sigma_{0,1} + \sin^2 \theta \sigma_{1,0} + 2 \sin \theta \cos \theta \sum_f |\sigma_{\text{int},f}| \cos(\Phi_f + \beta), \quad (\text{S27})$$

For identical particles, the total cross section becomes:

$$\sigma^{\text{ident}}(\theta, \beta) = \frac{|\cos \theta + \sin \theta e^{i\beta}|^2}{2} \sigma_{0,1}^s + \frac{|\cos \theta - \sin \theta e^{i\beta}|^2}{2} \sigma_{0,1}^a \quad (\text{S28})$$

The visibility of the control over the total cross section, evaluated at $\theta = \pi/4$ becomes:

$$V(\theta) = \frac{\sigma_{\text{max}}(\theta, \beta_{\text{max}}) - \sigma_{\text{min}}(\theta, \beta_{\text{min}})}{\sigma_{\text{max}}(\theta, \beta_{\text{max}}) + \sigma_{\text{min}}(\theta, \beta_{\text{min}})} = \frac{\left| \frac{\sigma_{01}^s}{\sigma_{01}^a} - 1 \right|}{\frac{\sigma_{01}^s}{\sigma_{01}^a} + 1} \quad (\text{S29})$$

For entangled superposition states, the visibility depends solely on the relative weight of the symmetric and anti-symmetric contributions. Importantly, it is no longer constrained by the satellite terms. In the ultracold regime, one of these contributions typically dominates over the other, enabling complete control of the total cross section. Thus, for entangled superpositions, full control of the total cross section at ultracold temperatures can be achieved for both identical fermions and identical bosons. This contrasts with the product-state case, where complete control is not attainable for identical bosons due to the presence of satellite terms.

Finally, for parity control, the parity contrast for identical fermion is

$$P(\beta) = \frac{|1 - e^{i\beta}|^2 \sigma_{01}^a - |1 + e^{i\beta}|^2 \sigma_{01}^s}{|1 + e^{i\beta}|^2 \sigma_{01}^a + |1 - e^{i\beta}|^2 \sigma_{01}^s} \quad (\text{S30})$$

which is equal to -1 (+1) for $\beta = 0(\pi)$. The parity switch index S_P defined in ?? is thus equal to 1, achieving complete control of parity. For identical bosons, the parities are permuted, but complete parity control is still maintained.

Figures S4 and S6 present the entangled initial state analogs of the results shown in the main text, which are presented using the entangled initial states.

Figure S4 shows the visibility for the control of the total cross section versus mixing angle θ for ${}^6\text{Li}+{}^6\text{Li}$, ${}^7\text{Li}+{}^7\text{Li}$, and ${}^6\text{Li}+{}^7\text{Li}$ at $T = 20 \mu\text{K}$. For the collisions of ${}^6\text{Li}+{}^6\text{Li}$, the visibility remains 1 across all control angles θ . In contrast to the limited maximum visibility of ~ 0.7 with the product initial state, ${}^7\text{Li}+{}^7\text{Li}$ shows complete control with visibility being 1 for all θ at $E = 20 \mu\text{K}$, since the removal of the satellite terms boosts the visibility, with detailed explanations in Figure S4. For ${}^6\text{Li}+{}^7\text{Li}$, although we see a slight increase of maximum visibility from 0.02 to ~ 0.05 , it is still much smaller than the analogs of the homonuclear cases. This is because for ${}^6\text{Li}+{}^7\text{Li}$, the asynchronization occurs even within each symmetry sector.

We observe the contrast of partial scattering cross sections with entangled initial states at $E = 20 \mu\text{K}$, as in Figure S4. For identical fermions, the figure looks like the one in the main text, since the satellite terms are naturally suppressed at ultracold temperatures. For identical bosons, the enhancement of the visibility for two identical bosons is shown clearly in panel (b), where only the symmetric components contribute to the total scattering cross section with the satellite term suppressed, thus causing the visibility to be 1.

Panel (c) clearly shows weak control for both populated final states, (8,0,0) and (12,0,0). This behavior originates from the partial distinguishability of the two interfering pathways and from the asymmetry of the corresponding transition cross sections. For the final state (8,0,0), the cross section from $|01\rangle$, $\sigma_{01 \rightarrow 8}$, is larger than that from $|10\rangle$, $\sigma_{10 \rightarrow 8}$. To enhance interference and thus

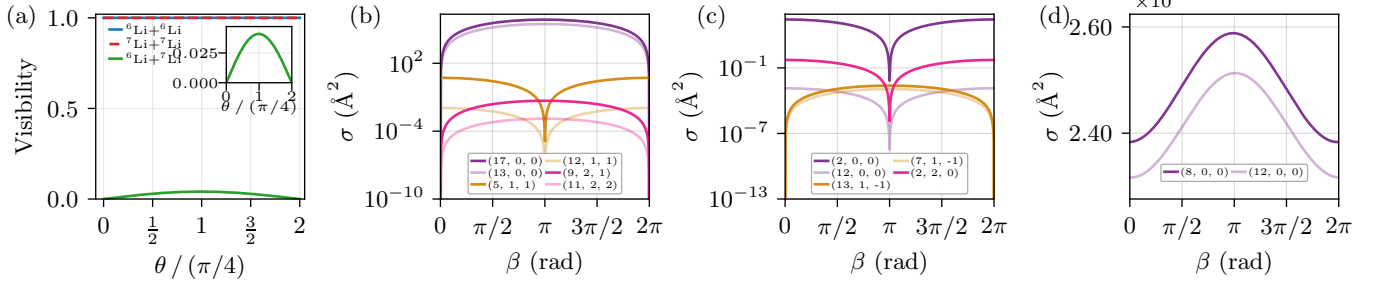


FIG. S4: (a) Visibility V of the total cross-section control versus θ for ${}^6\text{Li}+{}^6\text{Li}$, ${}^7\text{Li}+{}^7\text{Li}$, and ${}^6\text{Li}+{}^7\text{Li}$ with entangled initial state; the inset zooms in for ${}^6\text{Li}+{}^7\text{Li}$. (b)–(d): Dominant partial-wave-resolved state-to-state cross sections for (b) ${}^6\text{Li}+{}^6\text{Li}$, (c) ${}^7\text{Li}+{}^7\text{Li}$, and (d) ${}^6\text{Li}+{}^7\text{Li}$ with entangled initial state. Labels denote exit-channel quantum numbers $(\alpha_{\text{out}}, L_{\text{out}}, m_{L,\text{out}})$; colors indicate partial waves and opacity indicates hyperfine exit channels.

improve control, the amplitudes of the two pathways must be balanced. This would require increasing the population in the state $|10\rangle$, as illustrated by the blue curve in Fig. S5. In contrast, for the final state $(12,0,0)$, the asymmetry is reversed: $\sigma_{10\rightarrow 12}$ exceeds $\sigma_{01\rightarrow 12}$. Achieving balanced pathway contributions in this case would therefore require increasing the population in $|01\rangle$, as shown by the red curve in Fig. S5. Consequently, when considering the total cross section, it is impossible to simultaneously render the two pathways indistinguishable for both channels. This intrinsic incompatibility leads to the reduced visibility observed in the total cross section (Fig. S4). In particular, at $\theta = \pi/4$, Fig. S4 (d) shows weak control for both final states, reflecting the significant distinguishability of the two interfering pathways.

The energy dependence of the visibility is shown in Fig. S6. For ${}^6\text{Li}+{}^6\text{Li}$ and ${}^7\text{Li}+{}^7\text{Li}$, the introduction of the entangled initial state suppresses the contributions of the satellite terms at higher temperatures beyond the s-wave limit. Thus the maximum visibilities of the homonuclear cases get boosted between ~ 1 mK and 1K. Notice that now ${}^7\text{Li}+{}^7\text{Li}$ has complete controllability across wider regions, similar to ${}^6\text{Li}+{}^6\text{Li}$, until it reaches the energy of the p-wave centrifugal barrier near ~ 10 mK. For ${}^6\text{Li}+{}^7\text{Li}$, even though the satellite term is suppressed and the overall energy dependence of maximum visibility gets enhanced, the maximum visibility is still small across different collision energies because of the lack of synchronization of each state-to-state cross section.

6. IDENTICAL PARTICLE CASE WITH DIFFERENT STATES IN THE SUPERPOSITION OF THE TWO MOLECULES

Consider the scenario where the first molecule is prepared in a superposition of states $|0\rangle$ and $|1\rangle$ and the second molecule is prepared in a superposition of states $|1\rangle$ and $|2\rangle$:

$$\Psi_1 = \cos\theta|0\rangle + \sin\theta|1\rangle \quad (\text{S31})$$

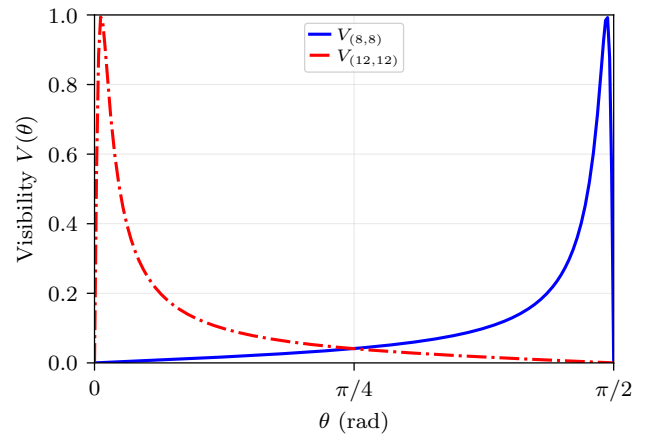


FIG. S5: Visibility $V(\theta)$ for the dominant state-to-state channels in the ${}^6\text{Li}+{}^7\text{Li}$ collision at $E = 2 \times 10^{-5}$ K as the mixing angle θ (which sets the relative populations of the two initial components $|01\rangle$ and $|10\rangle$) is varied. Because the single-path cross sections are asymmetric, the two channels require opposite population imbalances to balance the interfering amplitudes and thus enhance indistinguishability: for the final state $(8,0,0)$ one has $\sigma_{01\rightarrow 8} > \sigma_{10\rightarrow 8}$, so increased population in $|10\rangle$ (blue curve) is needed to maximize interference, whereas for $(12,0,0)$ the asymmetry is reversed, $\sigma_{10\rightarrow 12} > \sigma_{01\rightarrow 12}$, and increased population in $|01\rangle$ (red curve) is required. Consequently, the two channels cannot be optimized simultaneously, which limits the visibility in the total cross section; in particular, near $\theta = \pi/4$ (equal pathway weights) both channels exhibit weak control due to significant pathway distinguishability.

$$\Psi_2 = \cos\theta|1\rangle + \sin\theta e^{i\beta}|2\rangle \quad (\text{S32})$$

This kind of superposition was considered in our previous work on coherent control of ultracold collisions between O_2 molecules [S10]. The total internal state of the two-

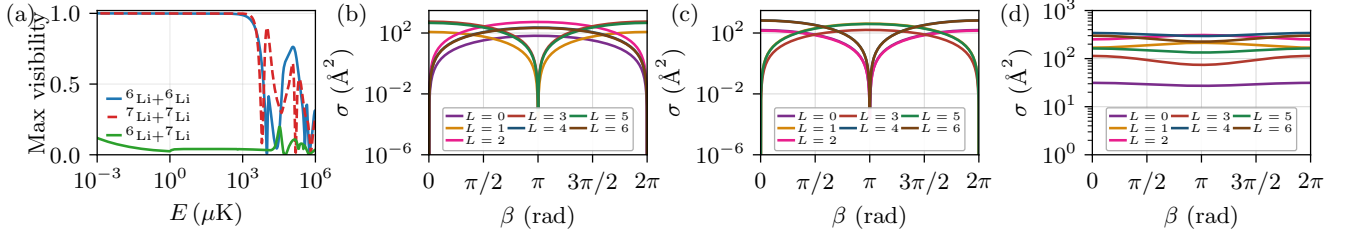


FIG. S6: (a): Maximum visibility V of the total cross-section control versus collision energy E for ${}^6\text{Li}+{}^6\text{Li}$, ${}^7\text{Li}+{}^7\text{Li}$, and ${}^6\text{Li}+{}^7\text{Li}$ with entangled initial states. (b)–(d): Total cross sections at different partial waves at $E = 1$ K with entangled initial states for (b) ${}^6\text{Li}+{}^6\text{Li}$, (c) ${}^7\text{Li}+{}^7\text{Li}$, and (d) ${}^6\text{Li}+{}^7\text{Li}$.

molecules in the symmetrized basis is:

$$\begin{aligned} \Psi_{ini} = & \frac{\cos^2 \theta}{\sqrt{2}} (|01\rangle_a + |01\rangle_s) + \frac{\cos \theta \sin \theta e^{i\beta}}{\sqrt{2}} (|02\rangle_a + |02\rangle_s) \\ & + \cos \theta \sin \theta |11\rangle + \frac{\sin^2 \theta e^{i\beta}}{\sqrt{2}} (|12\rangle_a + |12\rangle_s) \end{aligned} \quad (\text{S33})$$

The first notable difference is that the population of each component, given by the squared magnitude of its coefficient, is independent of the phase parameter β .

Second, interference effects can arise in the symmetrized basis. For instance, if the states are chosen such that $|02\rangle$ and $|11\rangle$ are degenerate in energy and share the same total projection of internal angular momentum (like in [S10]), then the states $|11\rangle$ and $|02\rangle_s$ can coherently interfere. Both states are symmetric under particle exchange and therefore scatter through the same set of partial waves (even for bosons and odd for fermions). In this case, the CCS matrix is no longer diagonal

The total cross section in this case becomes:

$$\begin{aligned} \sigma(\theta, \beta) = & \frac{\cos^4 \theta}{2} (\sigma_{01,a} + \sigma_{01,s}) + \frac{\cos^2 \theta \sin^2 \theta}{2} (\sigma_{02,a} + \sigma_{02,s}) \\ & + \cos^2 \theta \sin^2 \theta \sigma_{1,1} + \frac{\sin^4 \theta}{2} (\sigma_{12,a} + \sigma_{12,s}) \\ & + \frac{2}{\sqrt{2}} \sin^2 \theta \cos^2 \theta \sum_f |\sigma_{int,f}| \cos(\Phi_f + \beta), \end{aligned} \quad (\text{S34})$$

where $\sigma_{int,f} = \mathbf{C}_{02s,11}^{sup \rightarrow f}$.

Importantly, interference term between $|11\rangle$ and $|02\rangle_s$ is not constrained by exchange symmetry to be identical for all final states. Consequently, one recovers a situation analogous to the non-identical particle case, where the control parameters depends on the specific final state. Upon summation over final states, this leads to partial scrambling of the interference effects and a corresponding loss of global control.

The synchronization of the control across all final states, the main result of this work, requires one to use the initial superposition composed of the same internal eigenstates (Eqs.(1) and (2) of the main text).

7. BEHAVIORS OF STATE TO STATE CROSS SECTIONS AT HIGHER COLLISION ENERGIES

In this section, we analyze the mechanism responsible for the reduced control visibility of the total scattering cross sections shown in Fig. 4 of the main text. We show that, for identical particles, the loss of visibility arises primarily from the incoherent summation of contributions from different parity sectors. Within each symmetry sector, however, the control phases of the hyperfine state-to-state cross sections remain synchronized. In contrast, for distinguishable particles, phase scrambling occurs not only between different partial-wave parity sectors, but also within each sector, due to the absence of exchange symmetry.

As shown in Fig. S7, at 1 K many state-to-state cross sections contribute to the total scattering cross section with comparable magnitudes, making coherent control more difficult. For the homonuclear systems, ${}^6\text{Li}+{}^6\text{Li}$ and ${}^7\text{Li}+{}^7\text{Li}$, exchange symmetry constrains the relative phases of the state-to-state cross sections within a given parity sector. As a result, all contributions belonging to the same parity sector share the same control phase, independent of the specific final hyperfine state or partial wave. This phase synchronization is evident in panels (a) and (b). The total visibility is reduced only when even- and odd-parity contributions, which have different phases, are summed together.

The heteronuclear ${}^6\text{Li}+{}^7\text{Li}$ system behaves qualitatively differently. Because the particles are distinguishable, both even and odd partial waves are allowed for the same hyperfine entrance channel, and exchange symmetry no longer imposes phase constraints. Consequently, the relative phases of different state-to-state cross sections depend on both the final hyperfine channel and the partial wave (L, m_L), leading to both internal-state and partial-wave scrambling. This is clearly seen in panel (c): within a fixed partial wave sector, such as $L = 0$ or $L = 1$, different final internal states exhibit different control phases. Conversely, for a fixed final internal state, such as state 8, the control phase varies across different partial waves, including $L = 0, 1, 3, 4$, and 5. This behav-

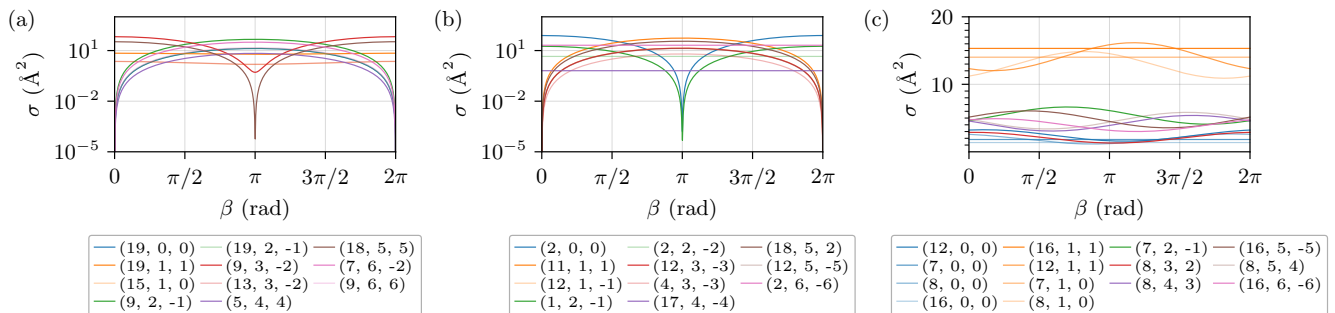


FIG. S7: Partial-wave-resolved state-to-state cross sections at $E = 1$ K for ${}^6\text{Li}+{}^6\text{Li}$, ${}^7\text{Li}+{}^7\text{Li}$, and ${}^6\text{Li}+{}^7\text{Li}$ with initial product state, shown from left to right. Labels denote exit-channel quantum numbers $(\alpha_{\text{out}}, L_{\text{out}}, m_{L,\text{out}})$; colors indicate partial waves and opacity indicates hyperfine exit channels.

ior is absent in the homonuclear cases, where all channels within the same parity sector remain phase synchronized.

Although the scattering systems considered here are specific to Li+Li collisions, the underlying mechanism is general. The principle of phase synchronization imposed by exchange symmetry for identical particles, and the corresponding phase scrambling for distinguishable particles, should also extend to more complex systems, including molecule–molecule collisions.

-
- [S1] E. Frishman, M. Shapiro, and P. Brumer, Optimized imploding waves in the coherent control of bimolecular processes: Atom-rotor scattering, *J. Phys. Chem. A* **103**, 10333 (1999).
- [S2] A. Devolder, T. V. Tscherbul, and P. Brumer, Interference is in the eye of the beholder: Application to the coherent control of collisional processes, *The Journal of Chemical Physics* **160**, 174304 (2024).
- [S3] W. Gunton, M. Semczuk, N. S. Dattani, and K. W. Madison, High-resolution photoassociation spectroscopy of the ${}^6\text{Li}_2$ $a(1^1\Sigma_u^+)$ state, *Phys. Rev. A* **88**, 062510 (2013).

- [S4] M. Semczuk, X. Li, W. Gunton, M. Haw, N. S. Dattani, J. Witz, A. K. Mills, D. J. Jones, and K. W. Madison, High-resolution photoassociation spectroscopy of the ${}^6\text{Li}_2$ $1^3\Sigma_g^+$ state, *Phys. Rev. A* **87**, 052505 (2013).
- [S5] J.-C. Zhang, P. Julienne, and Y. Liu, Characterization of feshbach resonances in a ${}^6\text{Li}-{}^7\text{Li}$ mixture using improved interaction potentials, *Phys. Rev. A* **113**, 062802 (2026).
- [S6] J. M. Hutson and C. R. Le Sueur, MOLSCAT: A program for non-reactive quantum scattering calculations on atomic and molecular collisions, *Computer Physics Communications* **241**, 9–18 (2019).
- [S7] A. Devolder, T. V. Tscherbul, and P. Brumer, Coherent control of ultracold molecular collisions: The role of resonances, *The Journal of Physical Chemistry Letters* **14**, 2171 (2023).
- [S8] M. Shapiro and P. Brumer, *Quantum control of Molecular Processes* (Wiley-VCH, 2012).
- [S9] A. Devolder, T. V. Tscherbul, and P. Brumer, Leveraging reactant entanglement in the coherent control of ultracold bimolecular chemical reactions, *Phys. Rev. Lett.* **135**, 233401 (2025).
- [S10] A. Devolder, P. Brumer, and T. V. Tscherbul, Complete quantum coherent control of ultracold molecular collisions, *Phys. Rev. Lett.* **126**, 153403 (2021).